CELL BIOLOGY

Overlap of NatA and IAP substrates implicates N-terminal acetylation in protein stabilization

Franziska Mueller[1], Alexandra Friese[1], Claudio Pathe[1]*, Richard Cardoso da Silva[1], Kenny Bravo Rodriguez[1], Andrea Musacchio[1,2†], Tanja Bange[1,3†]

SMAC/DIABLO and HTRA2 are mitochondrial proteins whose amino-terminal sequences, known as inhibitor of apoptosis binding motifs (IBMs), bind and activate ubiquitin ligases known as inhibitor of apoptosis proteins (IAPs), unleashing a cell's apoptotic potential. IBMs comprise a four-residue, loose consensus sequence, and binding to IAPs requires an unmodified amino terminus. Closely related, IBM-like N termini are present in approximately 5% of human proteins. We show that suppression of the N-alpha-acetyltransferase NatA turns these cryptic IBM-like sequences into very efficient IAP binders in cell lysates and in vitro and ultimately triggers cellular apoptosis. Thus, amino-terminal acetylation of IBM-like motifs in NatA substrates shields them from IAPs. This previously unrecognized relationship suggests that amino-terminal acetylation is generally protective against protein degradation in human cells. It also identifies IAPs as agents of a general quality control mechanism targeting unacetylated rogues in metazoans.

INTRODUCTION

As a protein's nascent chain emerges from a translating ribosome, its N terminus undergoes various modifications. Common are the acetylation of the initiator N-terminal methionine (Met^i) or its removal by methionine aminopeptidases (MetAPs) (*1*), followed by sequence-specific acetylation of the newly generated N terminus (*2*). N-terminal acetylation (Nt-Ac) may persist for the entire lifetime of the modified protein (*2*).

Nt-Ac requires acetyl–coenzyme A (CoA) as an acetyl donor, and an open question of general interest is the extent to which this modification is interwoven with metabolic regulation in different organisms (*3*, *4*). In a few well-studied cases, Nt-Ac has been implicated in cell physiological functions, including the stabilization of protein complexes, protein subcellular targeting, and protein aggregation (*2*). These functions of Nt-Ac may find an important level of convergence with pathways of regulated protein degradation. Early studies in human cells suggested that Nt-Ac may protect against protein degradation (*5*), and in selected cases, including the Hyx protein in *Drosophila melanogaster* and the THO complex subunit 7 (THOC7) protein in humans (*6*, *7*), a protective function of Nt-Ac has been documented.

More recent work, however, has questioned the role of Nt-Ac as a stabilizing marker. In *Saccharomyces cerevisiae*, acetylated protein N termini starting with methionine (Met or M), serine (Ser or S), alanine (Ala or A), threonine (Thr or T), or valine (Val or V) were proposed to act as potential degradation motifs (Ac-N-degrons). This pathway, which was proposed to predispose proteins for ubiquitin (Ub)–mediated proteolysis through the Doa10 and Not4 Ub-ligases (*8*, *9*), may be especially relevant in the context of protein quality control. A developing paradigm is that improper folding or abnormal stoichiometries of certain protein complex subunits cause exposure of the modified N termini, making them available for the degradation machinery (*8*). The generality of this mechanism, however, remains unclear (*10*).

Our interest in this problem stemmed from the specific question whether Nt-Ac influences processes of protein degradation during cell cycle progression and, more specifically, during mitosis. With an eye to the development of an experimental pipeline that would enable us to analyze variations in Nt-Ac in human cells, we began from a broader perspective and performed an unbiased analysis of the N-terminal proteome (N-terminome) of HeLa cells through mass spectrometry (MS)–based proteomics (*11*, *12*), building on, and extending, previous similar efforts (*12*–*16*). Starting from this dataset, we then developed a biochemical pipeline to identify putative interaction partners of naturally acetylated N-terminal motifs or of their unacetylated counterparts, which led to several unanticipated observations, as will be explained below. Our main general conclusion, corroborated by a remarkably consistent set of observations, is that the unacetylated versions of a large cohort of normally acetylated N termini targeted by the NatA acetyltransferase interact with E3 Ub ligases belonging to a family known as inhibitor of apoptosis proteins (IAPs). Collectively, our results are consistent with a crucial function of Nt-Ac in the control of protein stability. In agreement with previous observations obtained with a restricted number of proteins (*5*, *6*), our results suggest that Nt-Ac may play a general role in protein stabilization in human cells.

RESULTS AND DISCUSSION

The N-terminome of HeLa cells confirms the pervasiveness of Nt-acetylation

As discussed in detail in Methods and illustrated in fig. S1, we developed a pipeline for MS-based N-terminomics. Briefly, we used formaldehyde to dimethylate to completion all susceptible N termini in cleared HeLa cell lysates. The reaction spares preexisting acetylated N termini, on which methylation is ineffective, thus marking specifically unmodified or differently modified (e.g., unmodified or monomethylated) N termini. This allowed us to distinguish the latter

[1]Department of Mechanistic Cell Biology, Max Planck Institute of Molecular Physiology, Otto-Hahn-Str. 11, 44227 Dortmund, Germany. [2]Centre for Medical Biotechnology, Faculty of Biology, University Duisburg-Essen, Universitaetsstrasse, 45141 Essen, Germany. [3]Institute of Medical Psychology, Faculty of Medicine, LMU Munich.
*Present address: MRC Laboratory of Molecular Biology, Division of Protein and Nucleic Acid Chemistry, Francis Crick Avenue, Cambridge CB2 0QH, UK.
†Corresponding author. Email: andrea.musacchio@mpi-dortmund.mpg.de (A.M.); tanja.bange@med.uni-muenchen.de (T.B.)

from internal peptides created artificially by trypsin-mediated endoproteolysis at a later stage of the procedure. Internal peptides with intact N termini were selectively removed, and the resulting enriched preparations of N-terminal peptides were analyzed by high-resolution MS in a Q Exactive Plus Mass Spectrometer.

In line with previous studies (*11*, *13*–*15*, *17*), our results demonstrate the pervasiveness of Nt-Ac. Considering only peptides starting at position 1 (Met^i) or 2 (Met^i removed) of annotated protein sequences [UniProt (*18*)], we quantified N-terminal peptides in 2876 proteins (Fig. 1A and table S1). A total of 72.3% of these were fully N-terminally acetylated, 9.4% were partially acetylated, and 18.3% were dimethylated. As explained above and summarized in fig. S1, the "dimethylated peptide" group in our experimental setup gathers originally unmodified, monomethylated, and (if at all represented) dimethylated N termini, technically preventing an assessment of the prevalence of cellular N-terminal methylation.

Removal of Nt-acetylation promotes an interaction with IAP baculovirus IAP repeat domains

We reasoned that if Nt-Ac were part of N-terminal degradation signals (Nt-Ac-degrons), it ought to be a determinant of interactions with specialized receptors on Ub ligases or associated proteins. With the possible exception of MARCH6/TEB4 (the Doa10 ortholog), whether such receptors for Nt-Ac-degrons exist in humans is unclear. CDC20 is a well-established cell cycle regulator whose N terminus emerged from our analysis as being thoroughly N terminally acetylated (Fig. 1C). CDC20 is a coactivator of the anaphase-promoting complex/cyclosome (APC/C), an E3 Ub ligase required for the metaphase-anaphase transition (*19*). CDC20 presents the APC/C with two crucial targets, cyclin B and securin, whose degradation is required for eliciting this fundamental cell cycle transition. CDC20 stability is controlled at multiple levels during cell cycle progression (*19*), identifying this protein as a promising entry point in the study of the effects of Nt-Ac.

Because Nt-Ac has been previously shown to contribute directly to the stabilization of intramolecular interactions (*20*–*23*), we reasoned that we could use affinity chromatography to identify putative Nt-Ac-receptor(s) for CDC20. To this end, beads exposing acetylated or unacetylated synthetic peptides encompassing the N-terminal region of CDC20 were incubated with lysates of cycling HeLa cells, followed by MS-based quantification on retained binders (Fig. 1B). Defying our initial goal, no enrichment was observed with the acetylated version of the CDC20 peptide, with the exception of a few nonspecific binders (Fig. 1D and table S2). Conversely, the unmodified version of this peptide showed robust interactions with BIRC2, BIRC3, XIAP (X-linked IAP), and BIRC6 (also known as APOLLON or BRUCE), four members of an IAP family of E3 ubiquitin (Ub)–ligases that are key regulators of programmed cell death in development, tissue homeostasis, and tumorigenesis (*24*, *25*). Thus, our search for potential binding partners of CDC20's acetylated N-terminal region was inconclusive, but it suggested binding to IAPs E3 ligases as a possible outcome of defective acetylation.

To investigate the generality of these observations, we performed the same experiment with two additional peptides identified in our proteomic analysis as being fully acetylated, COMM domain-containing protein 10 (COMMD10) and deaminated glutathione amidase (NIT1). As negative controls, we used the N-terminal peptides from aspartate aminotransferase, cytoplasmic (GOT1) and 40S ribolomal protein S3a (RPS3A), whose sequences are related to those of COMMD10, NIT1, and CDC20 but that were measured as dimethylated (i.e., not acetylated; see above) in our screen (Fig. 1C). As for CDC20, the same four IAPs were strongly enriched in pull-down experiments with the unacetylated versions of the COMMD10 and NIT1 peptides, while no IAP enrichment was observed with the GOT1 or RPS3A control peptides (Fig. 1, E to G, and fig. S2A). Thus, three N-terminal peptides that are normally fully acetylated are also cryptic IAP binders whose IAP binding potential is unleashed when acetylation is missing, whereas the GOT1 and RPS3A peptides, which are not acetylated in vivo, are not cryptic IAP binders either. The glucose-induced degradation-deficient E3 ligase/C-terminal to LisH (hGID/CTLH) complex, a Ub-ligase implicated in the recognition of N-terminal proline (*26*, *27*), a residue that is never acetylated (*2*), was also enriched in pull-downs of the unacetylated COMMD10 peptide (table S2). The reason for this is unclear, but we speculate that it might reflect the unexpected exposure of Pro at position 3 in the COMMD10 peptide.

IAP family members comprise one to three 70-residue baculovirus IAP repeat (BIR) domains, but only BIRC2, BIRC3, and XIAP carry an additional RING domain that confers the Ub-ligase activity (*24*, *28*, *29*). BIRC6 has a Ub-conjugating (UBC) domain rather than a RING but has been shown to act as a chimeric E2/E3 Ub-ligase (*30*). Thus, the unacetylated forms of the COMMD10, NIT1, and CDC20 peptides pull down IAP family members with a proven activity as E3 ligases, whereas they do not pull down IAP family members, such as survivin, that are not associated with Ub-ligase activity (*31*).

The BIR domains of IAP Ub-ligases have been previously implicated in recognition of proteins containing a conserved inhibitor of apoptosis binding motif (IBM) in target proteins such as SMAC/DIABLO, caspase 9 (CASP9), and serine protease HTRA2, mitochondrial (HTRA2) considered crucial determinants of death pathway activation (*32*). Pull-down experiments from HeLa lysates with DIABLO, CASP9, or HTRA2 peptides identified the same four IAPs as preferential binding partners of the unacetylated peptides (Fig. 1, H to I, and fig. S2B), drawing a clear parallel with the COMMD10, NIT1, and CDC20 peptides.

The cryptic IBMs of COMMD10, NIT1, and CDC20 have sequence features that resemble those of the IBMs in SMAC/DIABLO, HTRA2, and CASP9 (Fig. 2A), suggesting that they bind the BIR domains. To test this, we asked whether unacetylated synthetic peptides encompassing the N termini of COMMD10, NIT1, and CDC20 interacted with representative BIR domains (fig. S3A), including the $BIRC3^{BIR3}$ domain and $XIAP^{Linker\text{-}BIR2\text{-}BIR3}$, a tandem BIR construct of XIAP also encompassing the so-called linker region, in a fluorescence polarization assay. The positive controls DIABLO and CASP9 IBM peptides and the COMMD10, NIT1, or CDC20 peptides bound to BIR domains with comparable dissociation constants (K_d), while none of the peptides bound to the $XIAP^{BIR1}$ domain, which does not interact with the IBMs of CASP9 and DIABLO (Fig. 2B, fig. S3B, and table S3) (*24*, *33*). Increasing amounts of DIABLO or COMMD10 peptides in solution competed with similar efficiency the pull-down of IAPs from cellular lysates by an immobilized biotinylated DIABLO peptide (fig. S4 and table S4). As expected on the basis of structural work on IBM:BIR complexes (*34*–*36*) and on our cell lysate pull-down experiments, Nt-Ac abrogated IAP binding by the COMMD10, NIT1, and CDC20 peptides (Fig. 2B and fig. S3B). The IAP-binding N termini of IBMs are generated posttranslationally by endoproteolysis (CASP9) or upon proteolytic processing of signal peptides during mitochondria

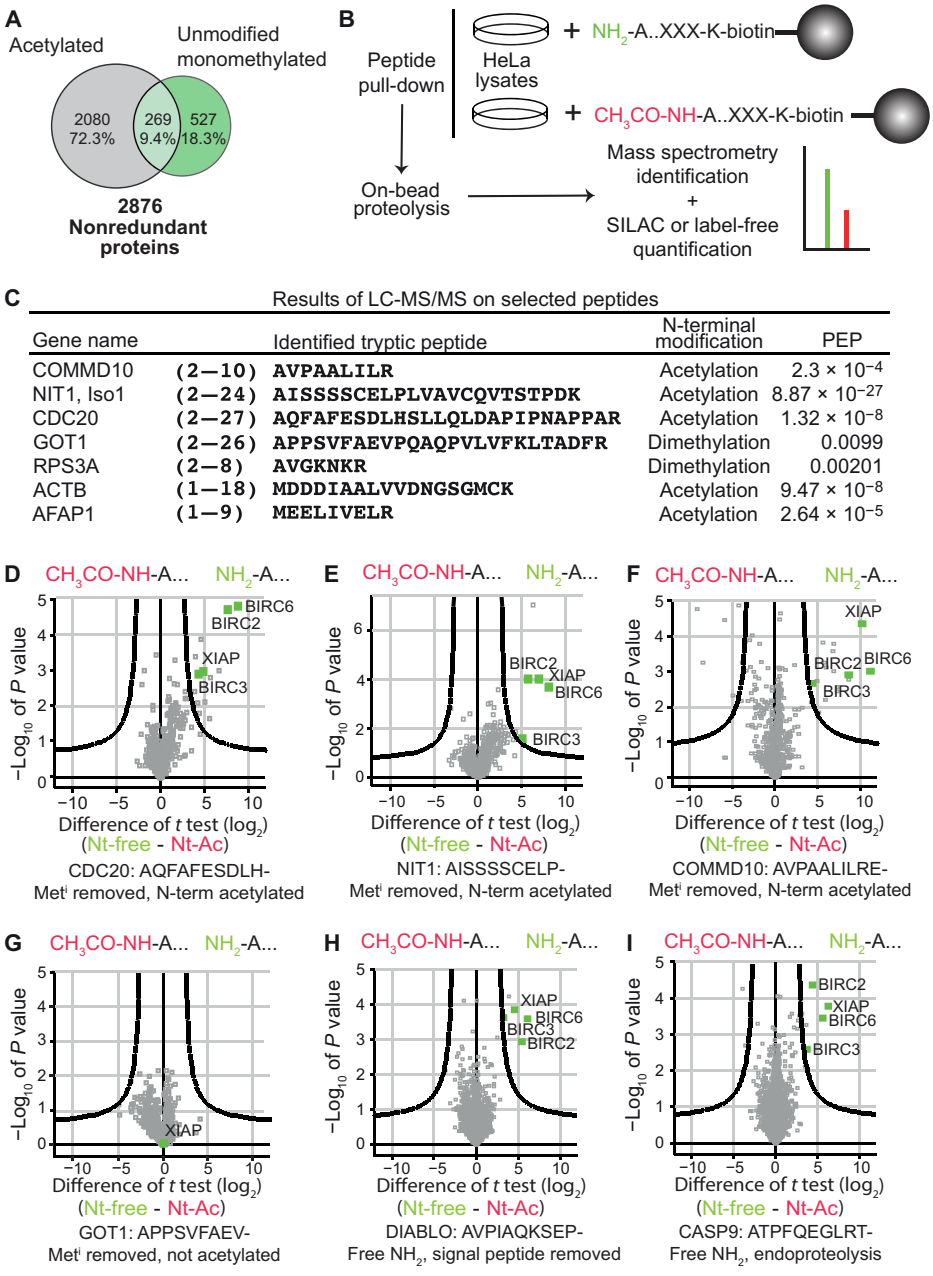

Fig. 1. Free Nt-α-amino forms of Nt-acetylated proteins bind to IAPs in cells. (**A**) Venn diagram summarizing numbers and percentages of all proteins with identified N termini from a large-scale MS experiment using HeLa cells (see experimental scheme in fig. S1). Total numbers and percentage of acetylated, dimethylated (reflecting unmodified, mono, and potentially also dimethylated N termini in cells), and proteins identified with both modifications are shown. All identified N termini are listed in detail in table S1. (**B**) Scheme of the performed peptide pull-down experiments. Nt-Ac or free Nt-α-amino (Nt-free) biotinylated peptides were bound to streptavidin beads. Beads were then incubated with HeLa lysates, washed, and directly digested on beads for MS analysis. Quantification was performed by using label-free intensities (label-free quantitation) or stable isotope labeling by amino acids in cell culture (SILAC). (**C**) Table of examples of N-terminal peptides from the MS dataset (A) used for pull-downs in 1(D to G) and fig. S2. Identified tryptic peptide, its N-terminal modification and posterior error probability (PEP) of the identification are specified. (**D** to **I**) Volcano plots from pull-down experiments comparing binders for free Nt-α-amino and Nt-Ac peptides from CDC20 (D), NIT1 (E), COMMD10 (F), and GOT1 (G) are shown. (**H** and **I**) The positive controls DIABLO and CASP9 are shown in (H) and (I), respectively. For all pull-downs the $-\log_{10}$ of the *t* test values (*y* axis) are plotted against the $\log_2$ of the fold difference of the *t* test (*x* axis) [*t* test, free Nt-α-amino (indicated as Nt-free) versus Nt-Ac; cutoff curve, false discovery rate (FDR) < 0.01, S0 > 2]. IAP family members are highlighted in green. LC-MS/MS, liquid chromatography–tandem MS.

insertion (SMAC/DIABLO and HTRA2), explaining why these sequences are not acetylated (*24*, *37*). Their regulated binding to IAPs results in ubiquitylation and degradation of their carriers (*24*). Collectively, these experiments indicate that IBMs and unacetylated cryptic IBM-like sequences of nuclear or cytosolic proteins bind to BIR domains with similar affinity.

The IBMs' first four residues are crucial for BIR domain binding (*34*–*36*). The first residue is generally alanine (A), but serine (S),

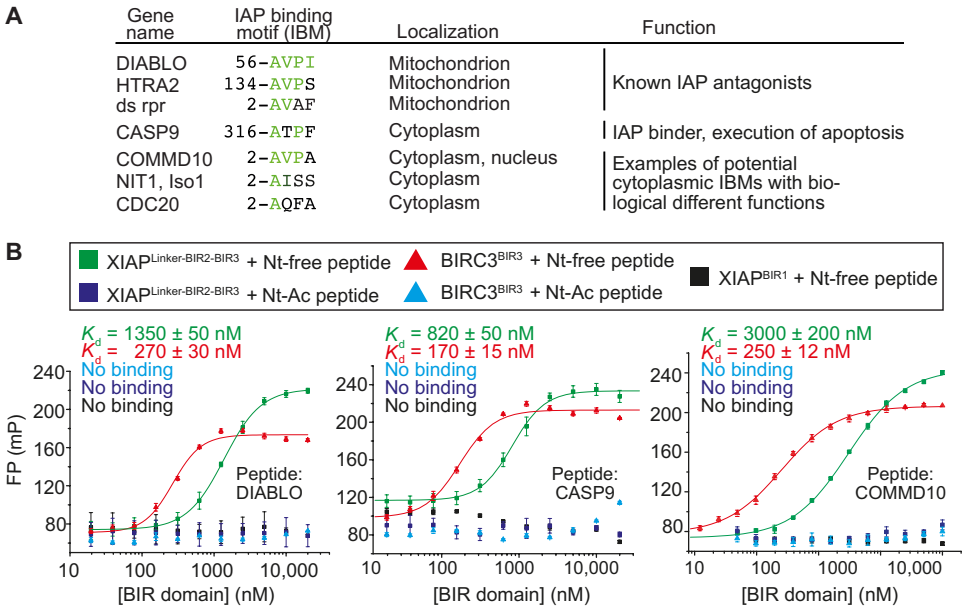

Fig. 2. Free Nt-α-amino peptides of cytosolic proteins bind to IAPs' BIR domains in vitro. (**A**) Table with examples of known IAP antagonists [DIABLO, HTRA2, and dr Reaper (rpr)], IAP binders (CASP9), and cytosolic proteins with potential N-terminal IBM motifs (COMMD10, NIT1 Isoform1, and CDC20). Gene name, (potential) IBM with N-terminal amino acid in processed protein, cellular localization, and function are shown. (**B**) Fluorescein isothiocyanate (FITC)–labeled peptides (free Nt-α-amino, indicated as Nt-free, or Nt-Ac, each used at a concentration of 20 nM) of DIABLO (left), CASP9 (middle), and COMMD10 (right) were incubated for 30 min with increasing concentrations of His-tag BIR domain constructs (XIAP$^{\text{Linker-BIR2-BIR3}}$, BIRC3$^{\text{BIR3}}$, or XIAP$^{\text{BIR1}}$). Fluorescence polarization (FP) was measured at excitation and emission wavelength of 470 and 525 nm and data (millipolarization units, mP) were plotted as a function of BIR domain concentration and fitted with a logistic fit using Origin7.0. K_d values are summarized in table S3. Measured combinations are shown schematically in the top panel.

valine (V), and threonine (T) are tolerated, and there is relatively modest sequence stringency at subsequent positions, although this may vary for different BIRs (*33*, *38*–*40*). Peptides with sequences retaining Met^1 [such as those of actin, cytoplasmic 1 (ACTB) and actin filament-associated protein 1 (AFAP1); Fig. 1C] or encompassing COMMD10 but with an N-terminal methionine that is normally processed did not enrich IAPs when exposed to HeLa lysates (fig. S2, C to F), suggesting that removal of the N-terminal methionine is prerequisite for IAP binding (albeit not sufficient, as shown by the GOT1 and RPS3A peptides). As previously noted (*33*), the incidence of IBM-like sequences in the human proteome is high (4285 sequences of 64,103 complete UniProt annotations were identified with an in-house developed program using the motif [AS]-[EVTQIDSMLFRG]-[PAGVCKMSR]-[VIDEFGLWAY], where square parentheses enclose single-letter codes of allowed residues at positions for residues 2 to 5).

Reduction of Nt-Ac generates new binding partners for IAPs

We asked whether the IAP-binding potential of cryptic IBMs could be unleashed by artificially reducing Nt-Ac in HeLa cells. Mammals have seven N-terminal acetyl transferases (NATs; designated as A to F and H) with different sequence specificities (*41*). NatA, which comprises catalytic NAA10 and regulatory NAA15 subunits, is the only NAT that recognizes peptide sequences starting with A, S, T, V, C, and G after removal of the initiator methionine (*2*, *42*), with the apparent exception of NatD, which is also able to target starting Ser but limited to histone H2A and H4 (*43*, *44*). NatA modifies ~40% of the proteome and is expected to target the majority if not all IBM-like motifs. We therefore targeted NatA by RNA interference (RNAi) for 48 hours (Fig. 3A) and additionally added MG132 for 3 hours before lysis to prevent possible proteasomal degradation of unacetylated targets after their ubiquitination by IAPs, a common fate of BIR domain binders (*28*, *29*). Lysates from RNAi- and mock-treated cells were used for pull-down experiments using His-tagged BIRC3$^{\text{BIR3}}$, XIAP$^{\text{Linker-BIR2-BIR3}}$, and XIAP$^{\text{BIR1}}$ as baits, and interaction partners were identified and quantified by MS. This analysis showed enrichment of several BIRC3$^{\text{BIR3}}$ and XIAP$^{\text{Linker-BIR2-BIR3}}$ binding partners from lysates of NatA RNAi–treated cells in comparison to lysates of mock-treated control cells. In the majority of cases, the enriched targets comprised proteins that (i) are Nt-acetylated under unperturbed conditions in our N-terminome dataset (table S1), (ii) are mainly annotated in UniProt as acetylated, and (iii) carry a cryptic IBM-like motif (fig. S5A and table S5). For a subset of proteins in this enriched set [displayed in green in Fig. 3 (B and C) and fig. S5 (B and C)], it was possible to sequence and quantify the free (i.e., unmodified) N-terminal peptide, thus allowing direct estimation of the enrichment of the non–Nt-acetylated form (free Nt-α-amino) in the BIRC3$^{\text{BIR3}}$ and XIAP$^{\text{Linker-BIR2-BIR3}}$ pull-downs. The enrichment was not caused by major changes in abundance of the target proteins, as no such changes were observed in whole-proteome measurements that readily detected reduced abundance of the NatA subunits caused by RNAi (fig. S5E and table S6). Thus, enrichment of IAP binders upon NatA depletion is likely caused by altered Nt-acetylation.

N-terminal peptides of proteins enriched on the XIAP$^{\text{BIR1}}$ pull-downs after NatA depletion, on the other hand, showed no obvious IBM-like motifs (Fig. 3, D and E; fig. S5, D and F to I; and table S5). The reason for their enrichment will therefore require further investigation, but we surmise that these binders represent abundant background proteins [e.g., ACTB/actin, which is known to be regulated by Nt-Ac (*45*–*47*)] whose unacetylated forms accumulate

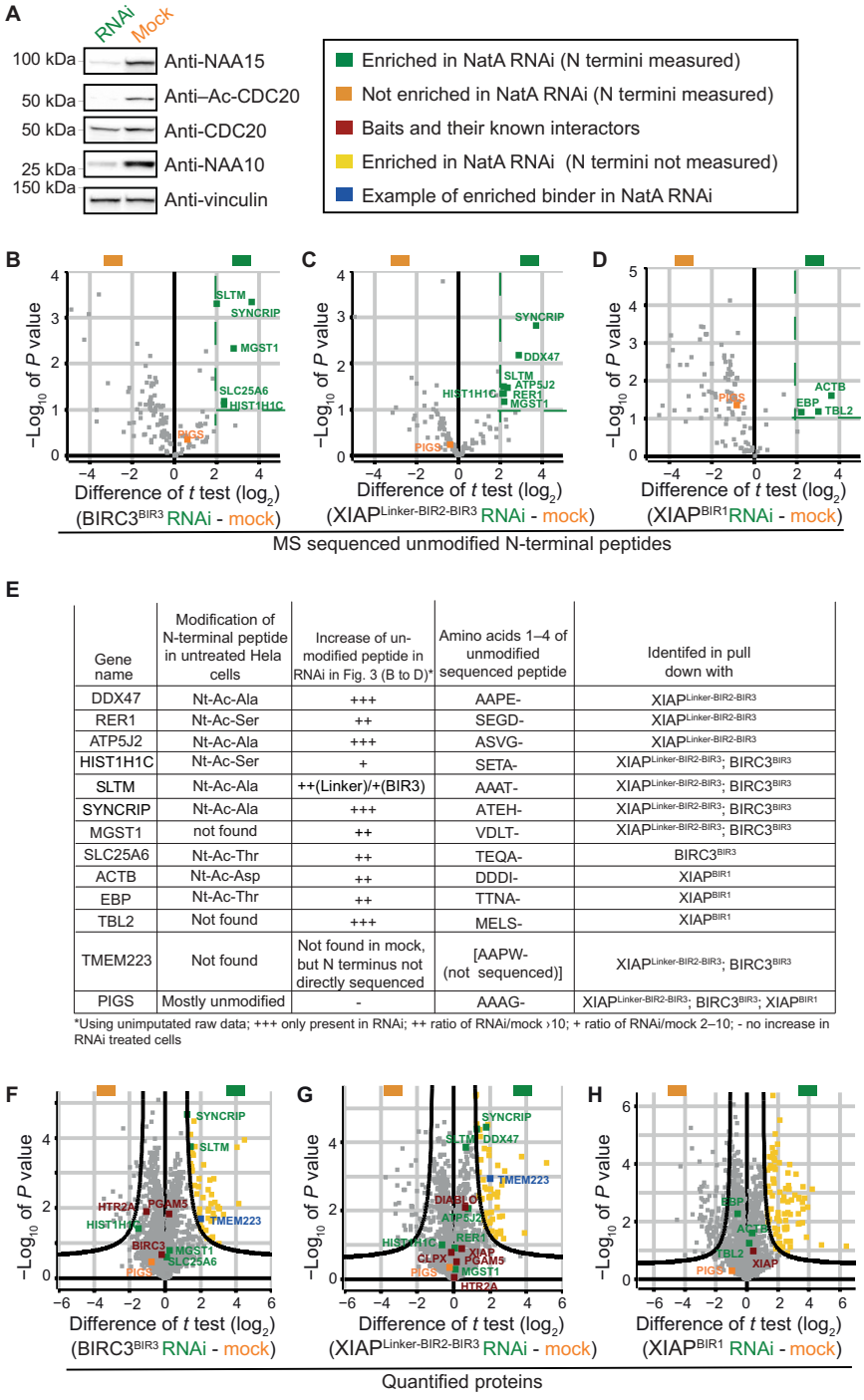

Gene name	Modification of N-terminal peptide in untreated Hela cells	Increase of un-modified peptide in RNAi in Fig. 3 (B to D)*	Amino acids 1–4 of unmodified sequenced peptide	Identifed in pull down with
DDX47	Nt-Ac-Ala	+++	AAPE-	XIAP$^{Linker-BIR2-BIR3}$
RER1	Nt-Ac-Ser	++	SEGD-	XIAP$^{Linker-BIR2-BIR3}$
ATP5J2	Nt-Ac-Ala	+++	ASVG-	XIAP$^{Linker-BIR2-BIR3}$
HIST1H1C	Nt-Ac-Ser	+	SETA-	XIAP$^{Linker-BIR2-BIR3}$; BIRC3^{BIR3}
SLTM	Nt-Ac-Ala	++(Linker)/+(BIR3)	AAAT-	XIAP$^{Linker-BIR2-BIR3}$; BIRC3^{BIR3}
SYNCRIP	Nt-Ac-Ala	+++	ATEH-	XIAP$^{Linker-BIR2-BIR3}$; BIRC3^{BIR3}
MGST1	not found	++	VDLT-	XIAP$^{Linker-BIR2-BIR3}$; BIRC3^{BIR3}
SLC25A6	Nt-Ac-Thr	++	TEQA-	BIRC3^{BIR3}
ACTB	Nt-Ac-Asp	++	DDDI-	XIAP^{BIR1}
EBP	Nt-Ac-Thr	++	TTNA-	XIAP^{BIR1}
TBL2	Not found	+++	MELS-	XIAP^{BIR1}
TMEM223	Not found	Not found in mock, but N terminus not directly sequenced	[AAPW- (not sequenced)]	XIAP$^{Linker-BIR2-BIR3}$; BIRC3^{BIR3}
PIGS	Mostly unmodified	-	AAAG-	XIAP$^{Linker-BIR2-BIR3}$; BIRC3^{BIR3}; XIAP^{BIR1}

*Using unimputated raw data; +++ only present in RNAi; ++ ratio of RNAi/mock ›10; + ratio of RNAi/mock 2–10; - no increase in RNAi treated cells

Fig. 3. BIR domains pull down proteins with free Nt-α-amino groups after NatA RNAi. (**A**) Left: Immunoblots (IBs) for NAA10, NAA15 (NatA subunits), Ac-CDC20, CDC20, and vinculin for RNAi-treated and mock-treated cells after 48 hours. "Mock" here and elsewhere means transfection without small interfering RNAs (siRNAs). Lysates were used for pull-downs in (B to D) and (F to H). Right: Legend of color coding for (B to D) and (F to H). (**B** to **D**) His-tag BIR domains BIRC3^{BIR3}, XIAP$^{Linker-BIR2-BIR3}$, and XIAP^{BIR1} were used to pull down proteins from HeLa lysates treated with RNAi for NatA or mock and 3 hours with MG132 before harvesting. Volcano plots for the quantified free Nt-α-amino peptides for BIRC3^{BIR3} (B), XIAP$^{Linker-BIR2-BIR3}$ (C), and XIAP^{BIR1} (D) are shown. Peptides enriched significantly in the NatA RNAi–treated samples are displayed in green (*t* test: $P < 0.1$, *t* test difference > 2); a control peptide from PIGS already known to be usually in the free Nt-α-amino form is colored in orange. (**E**) Table of proteins whose unmodified N-terminal peptides were specifically enriched in samples treated with RNAi for NatA [shown in (B to D)]. TMEM223, an example of a specific binder from the protein volcano plots [shown in (F and G)], and PIGS as nonspecific binder are also shown. Reported in the table are gene name, state of modification of the N-terminal peptide under unperturbed conditions (from N-terminome data; table S1), extent of enrichment of the unmodified N-terminal peptide in RNAi versus mock experiments extracted from the measured MS raw data, sequence of residues 1 to 4 of the N-terminal peptide measured in MS, and the bait used for the pull-down. (**F** to **H**) Volcano plots showing all quantified proteins (not limited to those whose N termini were directly sequenced) from the same pull-down experiments described in (B to D). Cutoff values: FDR < 0.05 and S0 > 1.

nonspecifically on the beads in the pull-downs from RNAi-treated cells.

For another cohort of enriched proteins, no direct information on Nt-Ac status was available. The existence of this cohort, however, suggests that additional specific binders of BIR domains are generated during NatA RNAi [yellow in Fig. 3 (F to H) and table S5]. In addition, for this cohort of targets, protein levels of significant binders remained, with only few exceptions, comparable in RNAi and mock samples, again suggesting that enrichment on BIR beads reflects a decrease in Nt-Ac (fig. S5E and table S6). The number of BIR-binding partners identified in these experiments is smaller than one may predict on the basis of the abundance of cryptic IBM-like sequences, but this likely reflects factors that include partial penetrance of the NatA RNA depletion, slow protein turnover limiting cotranslational generation of new and unacetylated N termini after depletion of NatA, and rapid protein degradation of unacetylated rogues during NatA depletion before addition of MG132. These considerations emphasize the importance of developing tools for the acute perturbation of Nt-acetylation.

Our hypothesis is that inhibition of NatA unleashes the IAP binding potential of IBM-like N termini. This hypothesis predicts that non–Nt-acetylated versions of $BIRC3^{BIR3}$ and $XIAP^{Linker\text{-}BIR2\text{-}BIR3}$ binders enriched after NatA RNAi (Fig. 3, B, C, and E) ought to retain IAPs from cell lysates similarly to other proteins studied in Fig. 1. We tested this with N-terminal peptides of SAFB-like transcription modulator (SLTM), probable ATP-dependent RNA helicase DDX47 (DDX47), ATP synthase subunit f (ATP5J2), and Transmembrane protein 223 (TMEM223) (Fig. 3; TMEM223 was included in these experiments because of a highly canonical IBM-like N-terminal sequence even if the acetylation status of its N terminus was unknown). As negative control for these experiments, we selected GPI transamidase component PIG-S (PIGS), a protein detected in pull-downs of all BIR domains but not showing NatA RNAi–dependent enrichment [in orange in Fig. 3 (B to D)]. The PIGS sequence starts with a more divergent IBM-like sequence that is mostly unacetylated under unperturbed conditions (Fig. 3E). Quantitative MS on pull-downs from HeLa lysates with acetylated or unacetylated N-terminal peptide pairs of the SLTM, DDX47, ATP5J2, and TMEM223 identified IAPs as binding partners of the unacetylated peptides. Conversely, no IAP enrichment was observed with the PIGS N-terminal peptide (Fig. 4, A to D; fig. S5J; and table S7). These results complement precisely the pull-down experiments in Fig. 3 and provide further evidence that lack of acetylation of proteins creates IBM-like motifs that mediate binding to IAPs.

Non–Nt-acetylated N termini are IAP substrates in vitro

Binding of agonists or antagonists to the BIR domains of IAPs activates their E3 Ub-ligase activity (*28*, *29*). We were therefore curious to assess whether cryptic IBMs identified in our analysis had the potential to activate the IAPs' ligase activity. For this analysis, we chose DDX47, whose non–Nt-acetylated form is a strong XIAP binder (Figs. 3C and 4B). We immunoprecipitated DDX47 from lysates of mock or NatA RNAi–treated HeLa cells additionally treated with MG132 for the last 3 hours before harvesting to prevent potential degradation of DDX47 by XIAP or other endogenous IAPs (Fig. 5B). In vitro ubiquitination assays with wild-type XIAP or with an inactive mutant (His467Ala) of XIAP showed DDX47 ubiquitination only on DDX47 precipitates from NatA RNAi–treated cells and in the

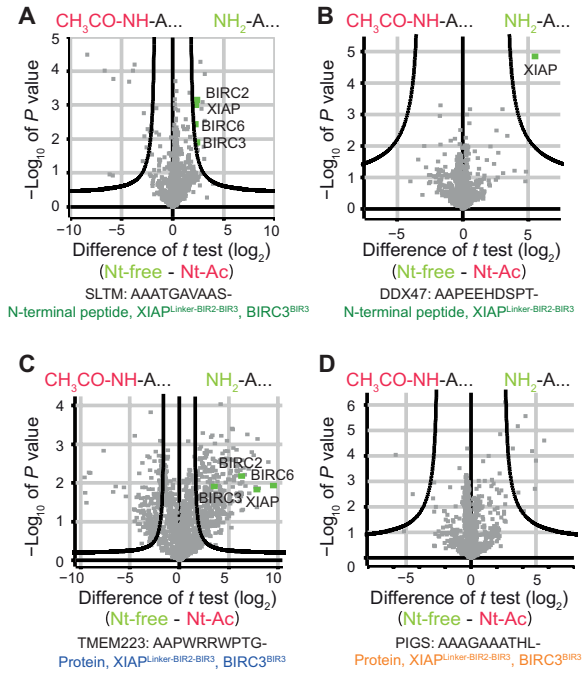

Fig. 4. Free Nt-α-amino peptides of new NatA substrates pull down IAPs from cell lysates. (**A** to **D**) Volcano plots from pull-down experiments comparing binders for free Nt-α-amino (Nt-free) and Nt-Ac peptides from SLTM (A) [green in Fig. 3 (B, C, F, and G)], DDX47 (B) [green in Fig. 3 (C and G)], TMEM223 (C) [blue in Fig. 3 (F and G)], and PIGS (D) as control [orange in Fig. 3 (B to D and F to H)] are shown. An FDR < 0.05 and S0 > 2 were applied for the cutoff curve. IAP family members are highlighted in green.

presence of wild-type XIAP, in agreement with the hypothesis that non–Nt-acetylated DDX47 turns into a XIAP substrate (Fig. 5C).

In a related experiment, we assumed that one or more lysine residues in the peptide-streptavidin complexes already used for lysate pull-downs in Fig. 1 might act as Ub acceptors of IAP ligases if these became enriched and activated upon their capture on beads. Therefore, we incubated pairs of unacetylated or acetylated N-terminal peptides of DIABLO, COMMD10, CASP9, and DDX47 bound to streptavidin beads with wild-type or inactive XIAP in in vitro ubiquitination assays. The non–Nt-acetylated COMMD10 and DDX47 bound to streptavidin were strongly ubiquitinated by XIAP, to levels that were comparable to those observed with the unacetylated DIABLO and CASP9 peptides (Fig. 5D). Acetylated peptides, unacetylated and acetylated peptides of PIGS (used as negative control), unconjugated streptavidin beads, and samples incubated with the ligase dead mutant of XIAP were not ubiquitinated, strongly indicating that agonist binding activates XIAP's activity.

Apoptosis induced by NatA knockdown requires IAPs

Apoptosis, triggered by activation of caspases, is the best-characterized programmed cell death pathway (*24*). In healthy cells, IAPs are believed to prevent unscheduled assembly of proapoptotic protein complexes by binding the IBMs of caspases, possibly sequestering them in an inactive form (*48*–*50*). Endogenous IAP antagonists and proapoptotic factors released from mitochondria, most notably SMAC/DIABLO, compete with caspases and displace them from the IAPs' BIR domains. This causes caspase activation and triggers downstream events in apoptosis, while also fuelling a positive feedback loop by

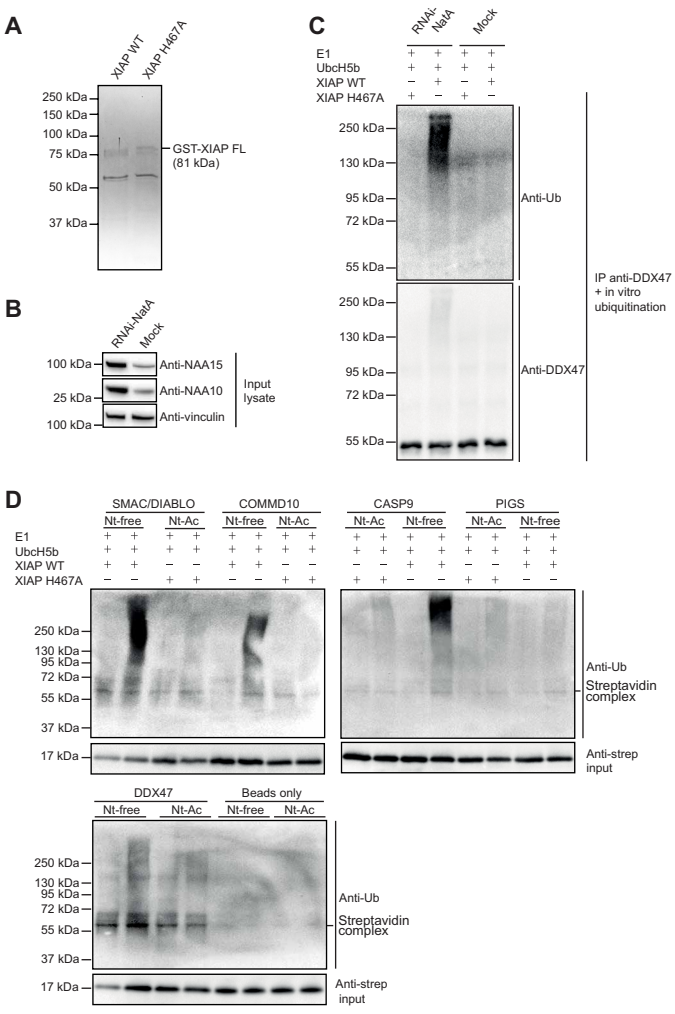

Fig. 5. XIAP ubiquitinates proteins and peptides with unmodified N termini. (**A**) Coomassie staining of purified wild-type or inactive (His467Ala) XIAP. (**B**) IBs of anti-NAA10, anti-NAA15, and anti-vinculin of input lysates used for DDX47 immunoprecipitations (IP) displayed in (C). (**C**) In vitro ubiquitination assay on DDX47 immunoprecipitates from HeLa cells treated for 48 hours with NatA RNAi or mock. In vitro ubiquitinations were performed as described in Methods using wild-type or mutant XIAP as E3 ligase. IBs of anti-ubiquitin and anti-DDX47 are shown. (**D**) Unacetylated and acetylated biotinylated peptides of DIABLO, COMMD10, CASP9, PIGS, and DDX47 bound to streptavidin beads were subjected to in vitro ubiquitination assays with wild-type or mutant XIAP. Streptavidin beads were used as additional control. Anti-ubiquitin and anti-streptavidin IBs are presented.

causing IAP down-regulation (*24*). Increased expression of IAPs is frequently observed in human cancers and is associated with treatment resistance, disease progression, and poor prognosis (*51*).

By forcing the generation of unacetylated IBM-like IAP binders, loss of NatA might be expected to promote proapoptotic conditions similar to those caused by release of endogenous IAP antagonists from mitochondria or by treatments with so-called SMAC mimetics, small-molecule competitors of the BIR-IBM interaction interface that may reactivate death pathways in resistant cells (*51*–*53*). Knockdown of NatA has been generally reported to reduce survival and cause apoptosis in cancer cell lines (*54*–*57*), but a protective effect from apoptosis has also been reported (*58*). We depleted NatA in HeLa cells by RNAi and performed flow cytometry analyses at 48 and 72 hours with annexin V and propidium iodide (PI) as markers. A total of 38.07 ± 4.42% cells were in apoptosis at 72 hours, showing a very significant increase compared to mock-treated cells (14.93 ± 1.31% apoptosis) (unpaired *t* test, $P = 0.0074$). This was comparable with the effects of a 4-hour treatment with staurosporine (38.53 ± 6.74% versus 7.75 ± 1.42%) (unpaired *t* test, $P = 0.0123$) (fig. S6A). On an IncuCyte reader, the apoptotic fraction of cells treated with RNAi of NatA versus mock steadily increased (unpaired *t* test for 44 hours, $P = 0.0007$) (fig. S6B). In addition, NatA RNAi led to increased poly(adenosine diphosphate–ribose) polymerase (PARP) cleavage, an indicator of apoptosis, after 72 hours. This effect was inhibited by the pan-caspase inhibitor Benzyloxycarbonyl-Val-Ala-Asp-fluoromethyl ketone (Z-VAD) (fig. S6C). Together, these observations indicate that reduction of NatA causes apoptosis.

Next, we wanted to assess whether apoptosis triggered by NatA knockdown required IAP activity. In the absence of additional apoptotic stimuli, we coupled RNAi-based depletion of NatA with RNAi-based depletion of XIAP, BIRC2, or both and assessed PARP cleavage after 48 or 72 hours. PARP cleavage appeared strongly increased at the 72-hour time point of NatA RNAi, although a slight increase was observed already after 48 hours. Concomitant depletion of XIAP, BIRC2, or both suppressed PARP cleavage (Fig. 6A). Thus, induction of apoptosis upon NatA depletion requires these IAPs.

NatA depletion caused a strong reduction in the levels of BIRC2 in various cancer cell lines (unpaired *t* test, $P = 0.0341$ for four repeats at 72-hour time point; Fig. 6, B and C) but notably less extensively in nontransformed RPE-1 cells. The extent of IAP depletion was comparable to that observed with the SMAC mimetic LCL161, a previously described effect believed to reflect activation of the IAPs' E3 ligase activity by IAP antagonists (*28*, *29*). With a Met^{i}-His N-terminal sequence, BIRC2 is predicted to escape methionine aminopeptidase and NatA activity, and it is therefore unlikely that NatA depletion creates a BIRC2 N-degron by itself. No comparable effect on IAP stability was observed upon depletion of the NAA20 subunit of NatB, which acetylates N termini with unrelated sequences (Fig. 6D) (*2*). Immunoprecipitations of green fluorescent protein (GFP)–BIRC2 from overexpressing stable cell lines demonstrated strong induction of BIRC2 ubiquitination after NatA RNAi and treatment with MG132 for 4 hours before cell harvesting, likely reflecting self-targeting. The activation of E3 ligase triggered by NatA depletion was comparable to that observed upon LCL161 treatment (Fig. 6E). These observations are consistent with the possibility that inhibition of NatA generates endogenous SMAC mimetics that cause activation and down-regulation of IAPs.

Conclusions

Here, we have uncovered a remarkable and previously unappreciated link that depicts Nt-Ac of NatA substrates as a general protective mark against IAP Ub-ligases, which have a proven record for targeting substrates for degradation (*24*, *25*). Our analysis provides mechanistic evidence to the idea that Nt-Ac in humans protects against protein degradation (*5*).

We anticipate that extensions of the methodology described here may lead to the identification and classification of additional N-terminal–binding proteins. While Nt-Ac is essentially universal in eukaryotes, the BIR-RING constellation of domains in IAPs does not appear to exist in *S. cerevisiae*. This suggests that recognition of

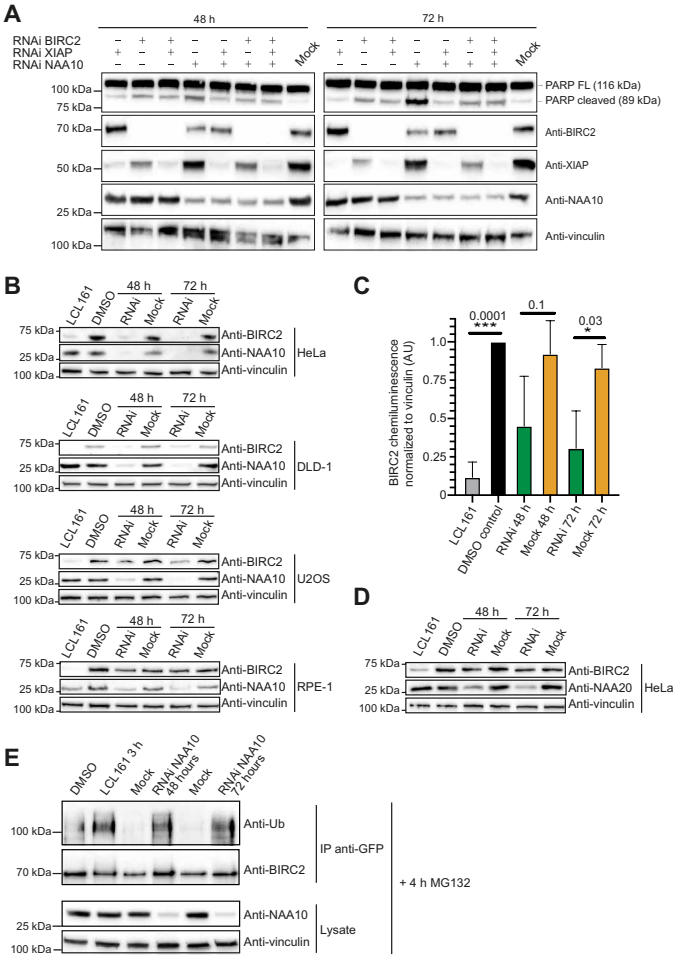

Fig. 6. RNAi of NatA triggers apoptosis in HeLa cells and requires IAPs. (**A**) NAA10 RNAi in HeLa cells was combined with RNAi of XIAP, BIRC2, or their combination, and HeLa cells were harvested after 48 (left) or 72 hours (right). Anti-PARP, anti-BIRC2, anti-XIAP, anti-NAA10, and anti-vinculin IBs are shown. (**B**) Lysates of HeLa, DLD-1, U2OS, and RPE-1 cells after treatment with or without the SMAC mimetic LCL161 for 20 hours or treated for NatA RNAi or mock for 48 or 72 hours. IBs against NAA10, BIRC2, and vinculin were performed. (**C**) Average levels of BIRC2 normalized to vinculin from four independent repeats of the indicated treatment in HeLa cells. Quantifications were performed with ImageJ (*72*). The dimethyl sulfoxide (DMSO) control for LCL161 was set to 100%, and unpaired *t* tests control versus treatment were performed: *P* value for LCL161 treatment, 0.0001; *P* value for NatA, 0.03. (**D**) HeLa cells were mock treated, treated with or without LCL161, or treated for NatB (NAA20) RNAi at 48 or 72 hours. IBs against NAA20, BIRC2, and vinculin were performed. (**E**) Immunoprecipitation of GFP-BIRC2 expressed from a stably transfected, expression-inducible HeLa cell line treated for NatA RNAi for 48 or 72 hours or mock treated or treated with LCL161 as control. All cells were treated with MG132 for 4 hours before harvesting to prevent protein degradation. Anti-ubiquitin and anti-BIRC2 IBs from immunoprecipitates and anti-NAA10 and anti-vinculin IBs from input cell lysates are shown. AU, arbitrary units.

unacetylated N termini on Ala, Ser, and other residues by IAPs is a more recent adaptation, possibly explaining why loss of NatA has modest effects on protein stability in *S. cerevisiae* (*10*). Previously, the N-end rule ligase Ubr1 and its orthologs have been proposed to act on the unacetylated variant of sequences starting with Met followed by a large hydrophobic residue (*59*).

Proteins with cryptic IBMs appear to form an extensive group in the human N-terminome. The N termini of these proteins are normally acetylated, contrarily to those of similar sequences that remain unacetylated because they are generated posttranslationally. While until now these unacetylated sequences have been exclusively considered in the context of pathways linked to apoptosis, our analysis suggests the possibility that IAPs, by targeting proteins that have not been acetylated, serve a more general role in protein quality control and sensing of metabolic energy, of which the NatA acetyl donor acetyl-CoA is a reporter (*60*). Two subunits associated with Cullin-RING Ub-ligases, ZYG11B and ZER1, have been proposed to function in an analogous quality control mechanism that operates after inhibition of myristoylation, a posttranslational modification of N-terminal glycines (Gly), and, additionally, in rapid degradation of cleavage products after activation of apoptosis (see Supplementary Discussion). The resulting unmodified N termini with Gly as first residue were shown to act as N-degrons through ZYG11B and ZER1 (*61*). Thus, proteins escaping their natural N-terminal modifications can undergo clearance through the Ub system. Future work will have to evaluate our hypothesis that this may be the primary function of IAPs.

METHODS

Reagents

Peptides were synthesized in-house or ordered from Mimotopes (Mulgrave, Victoria, Australia) or GenScript (Piscataway, NJ, USA). Peptide sequences were as follows: SMAC/DIABLO: Ac or H-AVPIAQKSEPFKKK-K(Biotin)-NH2, H-AVPIAQKSEPFKKK-K-(FITC-Ahx)-NH_2; CASP9: Ac or H-ATPFQEGLRTFKKK-K(Biotin)-NH_2; COMMD10: Ac or H-AVPAALILREKK-K(Biotin)-NH_2, H-AVPAALILREKKK-K-(FITC-Ahx)-NH_2, Ac, or H-MAVPAALILREKK-K(Biotin); CDC20: Ac or H-AQFAFESDLHSLLQL-PEG-K(Biotin)-$CONH_2$; NIT1: Ac or H-AISSSSCELPLVAVF-PEG-K(Biotin)-$CONH_2$; GOT1: Ac or H-APPSVFAEVPQAQPV-PEG-K(Biotin)-$CONH_2$; ACTB: Ac or H-MDDDIAALVVKKK-PEG-(Biotin) AFAP1: Ac or H-MEELIVELRLKKK-PEG-(Biotin); RPS3A: Ac or H-AVGKNKRLTKK-K-FITC; SLTM: Ac or H-AAATGAVAAS-KK-K-(Biotin)-NH_2; PIGS: Ac or H-AAAGAAATHLKK-K-(Biotin)-NH_2; TMEM223: Ac or H-AAPWRRWPTGKK-K-(Biotin)-NH_2; ATP5J2: Ac or H-ASVGECPAPVKK-K-(Biotin)-NH_2; DDX47: Ac or H-AAPEEHDSPTKK-K-(Biotin)-NH_2; and HTRA2: Ac or H-AVP-SPPPASPKK-K(Biotin). For peptide pull-downs, streptavidin beads (Streptavidin Sepharose High Performance, GE Healthcare, Chicago, IL, USA) were used: for His-tag pull-downs, magnetic beads (Dynabeads His-Tag Isolation and Pull-down, Invitrogen; 5 μl per pull-down) were used. For GFP pull-downs, GFP-Trap_A beads (ChromoTek GmbH, Planegg-Martinsried, Germany), and for Protein-G immunoprecipitation, Dynabeads Protein G (10003D, Thermo Fisher Scientific, Waltham, MA, USA) were used. Lysates were resuspended in sample buffer, boiled, and analyzed by SDS–polyacrylamide gel electrophoresis and immunoblotting using 10 or 12% tris/tricine gels blotted on nitrocellulose or polyvinylidene difluoride (PVDF) membrane. For immunoblots, the following antibodies were used: anti-AcCDC20 (in-house-made rabbit polyclonal antibody; 1:300 to 1000); for antibody generation, acetyl-AQFAFESDC-amide was conjugated to keyhole limpet hemocyanin and four rabbits were immunized with three to four boosts. Antibodies were affinity purified from serum on a column with the cross-linked antigen acetyl-AQFAFESDC. After elution, the purified antibody was affinity depleted on a column with AQFAFESDC-amid (antigen without acetylation). The flow-through of the affinity depletion was used to detect acetylated

CDC20. Other antibodies used in this work are as follows: anti-CDC20 (mouse monoclonal; 1:500; Santa Cruz Biotechnology, Dallas, TX, USA), anti-vinculin (mouse monoclonal; 1:20,000; Sigma-Aldrich, St. Louis, MO, USA), anti-NAA10 (PA5-32236, rabbit polyclonal; 1:5000; Thermo Fisher Scientific, Waltham, MA, USA), anti-NAA15 (PA5-30562, rabbit polyclonal; 1:10,000; Thermo Fisher Scientific, Waltham, MA, USA), anti-BIRC2 (ALX-803-335; 1:500, Enzo, New York, NY, USA), anti-BIRC3 (ALX-803-341; 1:500; Enzo, New York, NY, USA), anti-NAA20 (LS4C346227; 1:1000; LifeSpan BioSciences Inc., Seattle, WA, USA), anti-Ub horseradish peroxidase (HRP; sc-53509; 1:200; Santa Cruz Biotechnology, Dallas, TX, USA), anti-DDX47 (ab176852, Abcam plc; Discovery Drive, Cambridge Biomedical Campus, Cambridge, UK), and anti–GFP-HRP (ab190584; 1:10,000; Abcam plc, Discovery Drive, Cambridge Biomedical Campus, Cambridge, UK). Secondary antibodies anti-mouse (Amersham, Little Chalfont, UK), anti-rabbit (Amersham, Little Chalfont, UK), and anti-rat, all affinity-purified with HRP conjugate (working dilution, 1:10,000) or protein-G-HRP, were used. Images were acquired with the ChemiDoc MP Imaging System (Bio-Rad, Hercules, CA, USA). E1 (no. E-305), E2 (UBCH5B; no. E2-622), Ub (U-100H), Mg-ATP (no. B-20), and 10× E3 ligase reaction buffer (no. B-71) were purchased from Boston Biochem (Cambridge, MA, USA).

Cell culture and RNAi of NatA

HeLa, U2OS, DLD-1, or RPE-1 cells were grown in Dulbecco's minimum essential medium (DMEM; PAN-Biotech, Aidenbach, Germany) supplemented with 10% fetal bovine serum (Clontech, Kyoto, Japan) and 2 mM L-glutamine (PAN-Biotech, Aidenbach, Germany). For stable isotope labeling by amino acids in cell culture (SILAC), cells were cultivated for five passages in specialized SILAC medium (DMEM, E15-086; PAA, Cambridge, UK; dialyzed serum, A11-107, PAA, Cambridge, UK) supplemented with either "light" arginine and lysine (referred to as Arg-0 and Lys-0, A6969 and L8662; Sigma-Aldrich, St. Louis, MO, USA) or "heavy" arginine ($^{13}C_6{}^{15}N_4$) and lysine ($^{13}C_6{}^{15}N_2$) (referred to as Arg-10 and Lys-8) (*62*, *63*). For small interfering RNA (siRNA) transfections Lipofectamine RNAiMAX Transfection Reagent (Thermo Fisher Scientific, Waltham, MA, USA) was used at a final ratio of 1:333. SiNAA15_1 (CCAGAUGAAAUACUACUUCUU), siNAA15_2 (GAAGCUGCUGAAAUUUAUAUU) and/or siNAA10_1 (CUGACUGCGCCUUCACGAUUU) (all oligos from Sigma-Aldrich, St. Louis, MO, USA), siNAA20 (siRNA ID 111945), siXIAP (siRNA ID 121291), and siBIRC2 (siRNA ID S1448; all from Thermo Fisher Scientific, Waltham, MA, USA) were transfected at 25 nM each alone or in combination for 48 to 72 hours (*57*, *58*). Mock treatment is referred to transfection without siRNA. For pull-down experiments, 10 μM MG132 (Calbiochem, San Diego, USA) was added to the cells. The caspase inhibitor Z-VAD-FMK (G723B, Promega, Madison, USA) was added at 40 μM for 24 and 48 hours. To generate a stable HeLa cell line inducibly expressing enhanced green fluorescent protein (EGFP)–BIRC2, the Flp-In T-REx system (Invitrogen) was used.

Expression and purification of BIR domains and XIAP ligases

Expression vectors of human BIR domains (pET28b-XIAP-BIR1, pET28b-XIAP-Linker-BIR2-BIR3, pET21a-BIRC3-BIR3, and pGEX-XIAP fl) were a gift from M. Bolognesi and co-workers. Expression and purification of human BIR domains was performed as described (*64*). Briefly, proteins were expressed in *Escherichia coli* BL21(DE3) Codon$^+$RIPL cells in LB medium containing ampicillin or kanamycin for 16 to 20 hours at 18°C in the presence of 50 μM zinc acetate after induction with 0.2 mM isopropyl-β-D-thiogalactopyranoside. Cells were lysed by sonication in buffer containing 50 mM Hepes (pH 8.0), 250 mM NaCl, 5 mM dithioerythritol (DTE), and protease inhibitor cocktail (SERVA, Heidelberg, Germany). The cleared lysates were purified by affinity chromatography on HisTrap FF columns (GE Healthcare, Chicago, IL, USA), followed by size exclusion chromatography on Superdex 200 16/600 columns (GE Healthcare, Chicago, IL, USA) in buffer containing 20 mM Hepes (pH 8.0), 200 mM NaCl, and 5 mM DTE.

XIAP wild type and XIAP mutant His467Ala (done by QuikChange mutagenesis) were expressed in *E. coli* BL21(DE3) Codon$^+$RIPL cells in TB medium containing ampicillin for 16 to 20 hours at 20°C. Cells were lysed by passing through a fluidizer in buffer containing 50 mM Hepes (pH 7.5), 300 mM NaCl, 1 mM phenylmethylsulfonyl fluoride (PMSF), 10 mM imidazole, and 2 mM DTE. The cleared lysates were purified by affinity chromatography on HisTrap FF columns (GE Healthcare, Chicago, IL, USA), followed by a dialysis step overnight to the final buffer containing 50 mM Hepes (pH 7.5), 300 mM NaCl, and 2 mM DTE.

Fluorescence polarization

Fluorescein isothiocyanate (FITC)–labeled peptides (20 nM) were incubated with increasing concentrations of BIR domains in buffer containing 100 mM potassium phosphate (pH 7.5). For competition experiments, 5 nM FITC-labeled CASP9 peptide was mixed with 1.5 μM XIAP$^{\text{Linker-BIR2-BIR3}}$ or 0.5 μM BIRC3$^{\text{BIR3}}$ and increasing concentrations of unlabeled peptides. All experiments were performed in black, flat-bottomed 96-well microplates (Greiner Bio-One, Kremsmuenster, Austria). After 30-min incubation, fluorescence polarization was measured on a Tecan Safire 2 plate reader at excitation and emission wavelength of 470 and 525 nm, respectively. Fluorescence polarization data (millipolarization units, mP) were plotted as a function of BIR domain concentration or, for competition experiments, unlabeled peptide concentration and fitted with a logistic fit with Origin7.0 (www.originlab.com/doc/Origin-Help/Logistic-FitFunc).

Peptide pull-downs

Streptavidin beads were incubated with biotinylated peptides (10 μg of peptide/20 μl of slurry beads) for 30 min at room temperature in binding buffer A [150 mM NaCl, 50 mM tris (pH 8.0), and 0.075% NP-40]. Beads were washed once with lysis buffer [150 mM KCl, 75 mM Hepes (pH 7.5), 1.5 mM EGTA, 1.5 mM MgCl2, 10% glycerol, 1 mM dithiothreitol (DTT), and 0.1% NP-40] supplemented with protease inhibitor cocktail (SERVA, Heidelberg, Germany) and PhosSTOP phosphatase inhibitors (Roche, Basel, Switzerland). After washing, 1 mg of HeLa lysate in lysis buffer (2 mg/ml) was added to each sample. In case of competition assays, lysates were preincubated with different amounts (0 to 1000 μg) of FITC-labeled peptides for 2 hours at 4°C. Extracts were incubated with bound peptides on beads for 16 hours at 4°C. Pull-downs were washed twice with lysis buffer and twice with wash buffer (lysis buffer without NP-40, glycerol, DTT, inhibitor cocktail, and PhosSTOP phosphatase inhibitors). All experiments were performed at least in triplicate. Afterward, samples were transferred to new tubes and processed for MS analysis.

His-tag BIR domains pull-downs

Magnetic beads were saturated with His-tagged BIR-domains (BIRC3$^{\text{BIR3}}$, XIAP$^{\text{Linker-BIR2-BIR3}}$, and XIAP$^{\text{BIR1}}$) in binding buffer B

[50 mM potassium phosphate (pH 8.0), 300 mM NaCl, and 0.01% Tween 20] using a threefold excess over binding capacity for saturation. After 10 min of binding at 4°C, beads were washed once with binding buffer and afterward incubated for 1 hour at 4°C with 1 mg of lysate (mock-control or NatA-RNAi both treated for 3 hours with MG132 before harvesting) each in lysis buffer B (lysis buffer with only 0.075% NP-40). Pull-downs were washed once with lysis buffer and three times with wash buffer (lysis buffer without NP-40, glycerol, DTT, inhibitor cocktail, and PhosSTOP phosphatase inhibitors). All experiments were performed at least in triplicate. Afterward, samples were transferred to new tubes and prepared for MS analysis.

In vitro ubiquitination assays

E1 (50 nM), UBCH5B (250 nM), Ub (3 μg), Mg-ATP (3 mM), ligation buffer, and water were premixed. The premix was divided, and either XIAP WT or XIAP H467A (1 μM) was added. Premix (20 μl) was incubated with 10 μl of bead-bound substrate (final volume, 30 μl) for 1 hour at 30°C shaking. Samples were then washed four times with a buffer containing 50 mM Hepes (pH 7.5), 10% glycerol, 150 mM NaCl, 1% Triton, and 1 mM EDTA and loaded on a gradient gel (4 to 12%). Ubiquitination of substrates was assessed by immunoblot anti-Ub. Equal substrate loading was evaluated by immunoblotting against DDX47 or streptavidin. The immunoblots were as well incubated with anti-XIAP to be sure that it has been washed away after the reaction. DDX47 as substrate was prepared as follows: Dynabeads Protein G (10003D, Thermo Fisher Scientific, Waltham, MA, USA) have been used for binding 2 μg of anti-DDX47 antibody (ab176852, Abcam plc, Discovery Drive, Cambridge Biomedical Campus, Cambridge, UK) to 10 μl of slurry beads in phosphate-buffered saline (PBS) + 0.05% Tween 20 for 15 min at room temperature. After washing once with lysis buffer supplemented with protease inhibitor cocktail (SERVA, Heidelberg, Germany) and PhosSTOP phosphatase inhibitors (Roche, Basel, Switzerland), beads were incubated with 2.5 mg of HeLa lysate, either treated for 48 hours with siNAA10, siNAA15_1, and siNAA15_2 or mock control for 3 hours at 4°C. Cells had been treated with 10 μM MG132 3 hours before harvesting. After three washes with lysis buffer and supplements, immunoprecipitated DDX47 has been used as substrate for in vitro ubiquitination assays. Unacetylated and acetylated peptides of DIABLO, CASP9, COMMD10, DDX47, PIGS, and beads alone have been bound to streptavidin beads as for peptide pull-downs (10-fold molar excess peptide to beads), 1 to 2 μg of peptides have been used for each in vitro ubiquitination assay.

Immunoprecipitations

Stable inducible HeLa cell lines expressing EGFP-BIRC2 were treated for 48 or 72 hours with siNAA10 (or mock control) at 25 nM concentration including 4 hours of MG132 treatment. EGFP-BIRC2 expression was induced by addition of doxycycline (0.1 μg/ml; Sigma-Aldrich) for 24 hours. As control, cells were treated for 3 hours with 5 μM LCL161. GFP-Trap_A beads (20 μl; ChromoTek GmbH, Planegg-Martinsried, Germany) have been used for each pull-down and incubated with 500 μg of each lysate for 3 hours at 4°C in lysis buffer with supplements. After four washes in lysis buffer, 20 μl of 2× loading buffer was added to each sample and loaded to a 10% tris/tricine gel. Proteins were blotted to a PVDF membrane, afterward incubated for 30 min at 4°C in denature buffer [6 M guanidine-HCl, 20 mM tris-HCl (pH 7.5), 5 mM β-mercaptoethanol, and 1 mM PMSF], and, after washes in PBS, blocked in 5% bovine serum albumin in tris-buffered saline-Tween20 (TBS-T) for 6 hours at room temperature. Anti–Ub-HRP (sc-53509; 1:200; Santa Cruz Biotechnology, Dallas, TX, USA) was added overnight at 4°C.

Preparation of N-terminal peptides for MS analysis

Cells were lysed in Hepes buffer containing 8 M guanidine hydrochloride (GuHCl), Benzonase (90 U/ml), PhosSTOP phosphatase inhibitor, and protease inhibitor cocktail. Lysates were sonicated and centrifuged for 15 min at 5000*g* and 4°C. The supernatant was collected and clarified by ultracentrifugation (48000*g*, 20 min). The method was adopted from (*65*). Briefly, primary amines or monomethylated peptides were modified to dimethylated N termini. Purified proteins (1 mg) were transferred in 100 mM Hepes (pH 7.5) containing 4 M GuHCl. Proteins were reduced and alkylated. For dimethylation, formaldehyde was added to a final concentration of 40 mM. To avoid cross-linking between different amino acids (*66*) and ensure complete dimethylation of primary amines, 20 mM sodium cyanoborohydride ($NaBH_3CN$) were added immediately. pH was readjusted to 6 and 7, and proteins were incubated overnight at 37°C. The reaction was stopped by quenching formaldehyde with 100 mM ammonium bicarbonate. The pH was again adjusted to 6 and 7, and the dimethylated proteins were incubated for 4 hours at 37°C. Afterward, proteins were precipitated with acetone. Precipitated proteins were resuspended in 8 M GuHCl and then diluted 1:8 with 100 mM Hepes (pH 7.5). Proteins were digested with trypsin (1 μg per 50 μg of sample) at 37°C shaking overnight. Digested peptides were clarified by centrifugation at 10,000*g*, and a small portion was kept for MS analysis. The rest of the digested peptides were used for the enrichment of N-terminal peptides by depleting internal peptides from the mixture. The protocol is based on (*67*). Activated *N*-hydroxysuccinimide agarose beads (NHS beads; GE Healthcare) were used to covalently bind free N termini that became available through the tryptic digest and, thus, to enrich for modified real N termini. All reaction steps and centrifugations were done at 4°C. For the coupling, peptides were diluted in Na_2HPO_4 to a concentration of 0.5 mg/ml. For each milligram of sample, 5 ml of slurry beads were applied. NHS Sepharose were activated by washing two times with 1.5 ml of 1 M HCl and 1.5 ml of Na_2HPO_4, respectively. Peptides were coupled to NHS by incubating 4 hours at 4°C. Beads were spun down at 2000*g* for 1 min, and the supernatant was transferred on newly activated NHS beads and coupled for at least 8 hours as before. After the coupling, samples were centrifuged, and supernatants were collected. The remaining beads were washed once or twice again with one sample volume Na_2HPO_4 to collect all remaining unbound peptides. Peptides from input material, the dimethylation step, and N-terminal enrichment were measured by MS and analyzed altogether. The experiment was performed three times.

MS analysis

Samples were reduced, alkylated, digested either in solution (N termini measurements) or directly on beads (pull-down experiments) with LysC/Trypsin, and desalted/concentrated on C18-reversed phase stage tips as described (*68*). Obtained peptides were separated with a PepMap 100 RSLC C18 nano-HPLC column (2 μm, 100 Å, 75 ID × 25 cm; nanoViper, Dionex, Germany) on an UltiMate 3000 RSLCnano system (Thermo Fisher Scientific, Waltham, MA, USA) using a 125-min gradient from 5 to 60% acetonitrile with 0.1% formic acid and then directly sprayed via a nanoelectrospray source (Nanospray Flex Ion Source, Thermo Fisher Scientific, Waltham, MA, USA) in a Q Exactive Plus Hybrid Quadrupole-Orbitrap Mass Spectrometer (Thermo Fisher

Scientific, Waltham, MA, USA). The Q Exactive Plus was operated in a data-dependent mode acquiring one survey scan and subsequently 10 tandem MS (MS/MS) scans. A mass range of *m*/*z* 300 to 1650 was acquired with a resolution of 70,000 for full scan, followed by up to 10 high-energy collision dissociation MS/MS scans of the most intense at least doubly charged ions. Resulting raw files were processed with the MaxQuant software (version 1.5.2.18 or 1.6.1.13) searching against a UniProt human database (reference January 2016, 2018, or 2019) using oxidation (M) and acetylation (N terminus) as variable modifications and carbamidomethylation (C) as fixed modification (*69*). A false discovery rate (FDR) cutoff of 1% was applied at the peptide and protein level. The integrated label-free algorithm was used for relative quantification of proteins (*70*). For N-terminal analysis, we used dimethylation additionally as variable modification. Unmodified N termini and possible IBM-containing proteins were identified with the in-house app PeptideSearchTools (available at https://github.com/Kbr85/PeptideSearchTools). Unmodified N termini were searched considering only positions 1 and 2 of the proteins. IBM-containing proteins were identified using motif [AS]-[EVTQIDSMLFRG]-[PAGVCKMSR]-[VIDEFGLWAY] for residues 2 to 5 and considering only complete UniProt annotations.

Bioinformatic data analysis

Quantified proteins from full proteome measurement, peptide pull-downs, and His-tag pull-downs were further analyzed with Perseus (version 1.5.5.5. or 1.6.0.8) (*71*). Contaminant and reverse hits were removed, and label-free quantitation intensities were logarithmized. All experiments were at least done in triplicates, and proteins were required to be quantified in at least two of three replicates to be considered. SILAC experiments with RPS3A, ACTB, and AFAP1 were repeated at least twice with a label switch. Afterward, missing values were imputed at the lower end of the distribution of all measured and quantified proteins (down-shift, 1.8; width, 0.3). Specific interactors were identified with a Student's two-sample *t* test. Results were visualized with volcano plots (cutoffs were set to a permutation-based FDR between 0.01 and 0.05 for proteins and S0 between 1 and 2 depending on the experiment; for N-terminal peptides, a *t* test cutoff of 0.1 and at least fourfold difference between RNAi and untreated were chosen).

IncuCyte for apoptosis assay

HeLa cells were seeded into black-sided, clear-bottom 96-well plates (catalog no. 655090, Greiner Bio-One, Kremsmuenster, Austria) at approximately 50,000 cells per well. Cells were transfected with siNAA15_1, siNAA15_2, and siNAA10_1 as described above. To test apoptotic effects, cells were, at the same time, treated with CellEvent Caspase-3/7 Green Detection Reagent (catalog no. C10423, Invitrogen, Carlsbad, CA, USA) with a final concentration of 1 μM. Numbers of cells were detected by staining with NUCLEAR-ID Red DNA stain (catalog no. ENZ-52406, Enzo, New York, NY, USA) in parallel. All treatments were done at least in triplicate. Data from treated plates were collected with an IncuCyte ZOOM Live Cell Imaging device (Essen BioScience, Ann Arbor, MI, USA) and analyzed with the IncuCyte ZOOM control software. Cells were imaged every 2 hours for 48 hours. At each time point, four images were taken per well in bright-field, green (excitation/emission, 460 nm/524 nm), and red (excitation/emission 585/635 nm) channels. Images were analyzed for number of green objects per square millimeter and normalized for total cell number. Settings for this data collection were as follows: segmentation: "Top-Hat"; radius (μm), "30.000"; threshold (GCU), "3.0000"; "Edge Split On"; and edge sensitivity, "−20"; cleanup: hole fill (μm^2), "0.0000" and adjust size (pixels), "0"; filters: area (μm^2) min, "30.000."

Flow cytometry for apoptosis assay

The FITC Annexin V Apoptosis Detection Kit II (BD Pharmingen, San Diego, CA, USA) was used in this method. HeLa cells were transfected for 48 to 72 hours using 25 nM siNAA10_1 as described above. Control cells were induced to undergo apoptosis by treatment with staurosporine (300 nM, 4 hours). At the indicated time points, cells were trypsinized and washed twice with PBS and diluted in binding buffer C [10 mM Hepes/NaOH (pH 7.4), 140 mM NaCl, and 2.5 mM $CaCl_2$] to around 1×10^6 cells/ml. A total of 1×10^5 cells (100 μl) were incubated with FITC annexin V and PI. For setting up compensation and quadrants, unstained cells and cells stained only with FITC annexin V or only with PI were used as controls. After 15 min of incubation at room temperature in the dark, cells were diluted 1:5 in binding buffer and analyzed by flow cytometry (BD Accuri C6 Flow Cytometer, Franklin Lakes, NJ, USA).

SUPPLEMENTARY MATERIALS

Supplementary material for this article is available at http://advances.sciencemag.org/cgi/content/full/7/3/eabc8590/DC1

View/request a protocol for this paper from *Bio-protocol*.

REFERENCES AND NOTES

1. Q. Xiao, F. Zhang, B. A. Nacev, J. O. Liu, D. Pei, Protein N-terminal processing: Substrate specificity of *Escherichia coli* and human methionine aminopeptidases. *Biochemistry* **49**, 5588–5599 (2010).
2. H. Aksnes, R. Ree, T. Arnesen, Co-translational, post-translational, and non-catalytic roles of N-terminal acetyltransferases. *Mol. Cell* **73**, 1097–1114 (2019).
3. S. Varland, H. Aksnes, F. Kryuchkov, F. Impens, D. Van Haver, V. Jonckheere, M. Ziegler, K. Gevaert, P. Van Damme, T. Arnesen, N-terminal acetylation levels are maintained during acetyl-CoA deficiency in *Saccharomyces cerevisiae*. *Mol. Cell. Proteomics* **17**, 2309–2323 (2018).
4. C. H. Yi, H. Pan, J. Seebacher, I.-H. Jang, S. G. Hyberts, G. J. Heffron, M. G. V. Heiden, R. Yang, F. Li, J. W. Locasale, H. Sharfi, B. Zhai, R. Rodriguez-Mias, H. Luithardt, L. C. Cantley, G. Q. Daley, J. M. Asara, S. P. Gygi, G. Wagner, C.-F. Liu, J. Yuan, Metabolic regulation of protein N-alpha-acetylation by Bcl-xL promotes cell survival. *Cell* **146**, 607–620 (2011).
5. A. Hershko, H. Heller, E. Eytan, G. Kaklij, I. A. Rose, Role of the alpha-amino group of protein in ubiquitin-mediated protein breakdown. *Proc. Natl. Acad. Sci. U.S.A.* **81**, 7021–7025 (1984).
6. L. M. Myklebust, P. Van Damme, S. I. Støve, M. J. Dörfel, A. Abboud, T. V. Kalvik, C. Grauffel, V. Jonckheere, Y. Wu, J. Swensen, H. Kaasa, G. Liszczak, R. Marmorstein, N. Reuter, G. J. Lyon, K. Gevaert, T. Arnesen, Biochemical and cellular analysis of Ogden syndrome reveals downstream Nt-acetylation defects. *Hum. Mol. Genet.* **24**, 1956–1976 (2015).
7. S. Goetze, E. Qeli, C. Mosimann, A. Staes, B. Gerrits, B. Roschitzki, S. Mohanty, E. M. Niederer, E. Laczko, E. Timmerman, V. Lange, E. Hafen, R. Aebersold, J. Vandekerckhove, K. Basler, C. H. Ahrens, K. Gevaert, E. Brunner, Identification and functional characterization of N-terminally acetylated proteins in *Drosophila melanogaster*. *PLOS Biol.* **7**, e1000236 (2009).
8. A. Shemorry, C.-S. Hwang, A. Varshavsky, Control of protein quality and stoichiometries by N-terminal acetylation and the N-end rule pathway. *Mol. Cell* **50**, 540–551 (2013).
9. C.-S. Hwang, A. Shemorry, A. Varshavsky, N-terminal acetylation of cellular proteins creates specific degradation signals. *Science* **327**, 973–977 (2010).
10. I. Kats, A. Khmelinskii, M. Kschonsak, F. Huber, R. A. Knieß, A. Bartosik, M. Knop, Mapping degradation signals and pathways in a Eukaryotic N-terminome. *Mol. Cell* **70**, 488–501.e5 (2018).
11. N. Mischerikow, A. J. Heck, Targeted large-scale analysis of protein acetylation. *Proteomics* **11**, 571–589 (2011).
12. P. Van Damme, T. Arnesen, K. Gevaert, Protein alpha-N-acetylation studied by N-terminomics. *FEBS J.* **278**, 3822–3834 (2011).
13. P. Van Damme, M. Lasa, B. Polevoda, C. Gazquez, A. Elosegui-Artola, D. S. Kim, E. De Juan-Pardo, K. Demeyer, K. Hole, E. Larrea, E. Timmerman, J. Prieto, T. Arnesen, F. Sherman, K. Gevaert,

R. Aldabe, N-terminal acetylome analyses and functional insights of the N-terminal acetyltransferase NatB. *Proc. Natl. Acad. Sci. U.S.A.* **109**, 12449–12454 (2012).
14. P. F. Lange, P. F. Huesgen, C. M. Overall, TopFIND 2.0–-Linking protein termini with proteolytic processing and modifications altering protein function. *Nucleic Acids Res.* **40**, D351–D361 (2012).
15. W. V. Bienvenut, D. Sumpton, A. Martinez, S. Lilla, C. Espagne, T. Meinnel, C. Giglione, Comparative large scale characterization of plant *versus* mammal proteins reveals similar and idiosyncratic *N*-α-acetylation features. *Mol. Cell. Proteomics* **11**, M111.015131 (2012).
16. A. O. Helbig, S. Rosati, P. W. W. M. Pijnappel, B. van Breukelen, M. H. T. H. Timmers, S. Mohammed, M. Slijper, A. J. R. Heck, Perturbation of the yeast N-acetyltransferase NatB induces elevation of protein phosphorylation levels. *BMC Genomics* **11**, 685 (2010).
17. T. Arnesen, P. Van Damme, B. Polevoda, K. Helsens, R. Evjenth, N. Colaert, J. E. Varhaug, J. Vandekerckhove, J. R. Lillehaug, F. Sherman, K. Gevaert, Proteomics analyses reveal the evolutionary conservation and divergence of N-terminal acetyltransferases from yeast and humans. *Proc. Natl. Acad. Sci. U.S.A.* **106**, 8157–8162 (2009).
18. The UniProt Consortium, UniProt: A worldwide hub of protein knowledge. *Nucleic Acids Res.* **47**, D506–D515 (2019).
19. H. Yamano, APC/C: Current understanding and future perspectives. *F1000Res* **8**, F1000 (2019).
20. Z. Zhang, K. Kulkarni, S. J. Hanrahan, A. J. Thompson, D. Barford, The APC/C subunit Cdc16/Cut9 is a contiguous tetratricopeptide repeat superhelix with a homo-dimer interface similar to Cdc27. *EMBO J.* **29**, 3733–3744 (2010).
21. D. C. Scott, J. T. Hammill, J. Min, D. Y. Rhee, M. Connelly, V. O. Sviderskiy, D. Bhasin, Y. Chen, S.-S. Ong, S. C. Chai, A. N. Goktug, G. Huang, J. K. Monda, J. Low, H. S. Kim, J. A. Paulo, J. R. Cannon, A. A. Shelat, T. Chen, I. R. Kelsall, A. F. Alpi, V. Pagala, X. Wang, J. Peng, B. Singh, J. W. Harper, B. A. Schulman, R. K. Guy, Blocking an N-terminal acetylation-dependent protein interaction inhibits an E3 ligase. *Nat. Chem. Biol.* **13**, 850–857 (2017).
22. D. C. Scott, J. K. Monda, E. J. Bennett, J. W. Harper, B. A. Schulman, N-terminal acetylation acts as an avidity enhancer within an interconnected multiprotein complex. *Science* **334**, 674–678 (2011).
23. J. K. Monda, D. C. Scott, D. J. Miller, J. Lydeard, D. King, J. W. Harper, E. J. Bennett, B. A. Schulman, Structural conservation of distinctive N-terminal acetylation-dependent interactions across a family of mammalian NEDD8 ligation enzymes. *Structure* **21**, 42–53 (2013).
24. J. Silke, P. Meier, Inhibitor of apoptosis (IAP) proteins-modulators of cell death and inflammation. *Cold Spring Harb. Perspect. Biol.* **5**, a008730 (2013).
25. D. Vucic, V. M. Dixit, I. E. Wertz, Ubiquitylation in apoptosis: A post-translational modification at the edge of life and death. *Nat. Rev. Mol. Cell Biol.* **12**, 439–452 (2011).
26. F. Lampert, D. Stafa, A. Goga, M. V. Soste, S. Gilberto, N. Olieric, P. Picotti, M. Stoffel, M. Peter, The multi-subunit GID/CTLH E3 ubiquitin ligase promotes cell proliferation and targets the transcription factor Hbp1 for degradation. *eLife* **7**, e35528 (2018).
27. S.-J. Chen, X. Wu, B. Wadas, J.-H. Oh, A. Varshavsky, An N-end rule pathway that recognizes proline and destroys gluconeogenic enzymes. *Science* **355**, eaal3655 (2017).
28. E. Varfolomeev, J. W. Blankenship, S. M. Wayson, A. V. Fedorova, N. Kayagaki, P. Garg, K. Zobel, J. N. Dynek, L. O. Elliott, H. J. A. Wallweber, J. A. Flygare, W. J. Fairbrother, K. Deshayes, V. M. Dixit, D. Vucic, IAP antagonists induce autoubiquitination of c-IAPs, NF-κB activation, and TNFα-dependent apoptosis. *Cell* **131**, 669–681 (2007).
29. J. E. Vince, W. W.-L. Wong, N. Khan, R. Feltham, D. Chau, A. U. Ahmed, C. A. Benetatos, S. K. Chunduru, S. M. Condon, M. M. Kinlay, R. Brink, M. Leverkus, V. Tergaonkar, P. Schneider, B. A. Callus, F. Koentgen, D. L. Vaux, J. Silke, IAP antagonists target cIAP1 to induce TNFα-dependent apoptosis. *Cell* **131**, 682–693 (2007).
30. T. Bartke, C. Pohl, G. Pyrowolakis, S. Jentsch, Dual role of BRUCE as an antiapoptotic IAP and a chimeric E2/E3 ubiquitin ligase. *Mol. Cell* **14**, 801–811 (2004).
31. J. Silke, D. L. Vaux, Two kinds of BIR-containing protein - inhibitors of apoptosis, or required for mitosis. *J. Cell Sci.* **114**, 1821–1827 (2001).
32. S. M. Srinivasula, R. Hegde, A. Saleh, P. Datta, E. Shiozaki, J. Chai, R.-A. Lee, P. D. Robbins, T. Fernandes-Alnemri, Y. Shi, E. S. Alnemri, A conserved XIAP-interaction motif in caspase-9 and Smac/DIABLO regulates caspase activity and apoptosis. *Nature* **410**, 112–116 (2001).
33. M. C. Sweeney, X. Wang, J. Park, Y. Liu, D. Pei, Determination of the sequence specificity of XIAP BIR domains by screening a combinatorial peptide library. *Biochemistry* **45**, 14740–14748 (2006).
34. Z. Liu, C. Sun, E. T. Olejniczak, R. P. Meadows, S. F. Betz, T. Oost, J. Herrmann, J. C. Wu, S. W. Fesik, Structural basis for binding of Smac/DIABLO to the XIAP BIR3 domain. *Nature* **408**, 1004–1008 (2000).
35. G. Wu, J. Chai, T. L. Suber, J.-W. Wu, C. Du, X. Wang, Y. Shi, Structural basis of IAP recognition by Smac/DIABLO. *Nature* **408**, 1008–1012 (2000).
36. J. Chai, C. du, J.-W. Wu, S. Kyin, X. Wang, Y. Shi, Structural and biochemical basis of apoptotic activation by Smac/DIABLO. *Nature* **406**, 855–862 (2000).
37. W. Neupert, J. M. Herrmann, Translocation of proteins into mitochondria. *Annu. Rev. Biochem.* **76**, 723–749 (2007).
38. M. C. Franklin, S. Kadkhodayan, H. Ackerly, D. Alexandru, M. D. Distefano, L. O. Elliott, J. A. Flygare, G. Mausisa, D. C. Okawa, D. Ong, D. Vucic, K. Deshayes, W. J. Fairbrother, Structure and function analysis of peptide antagonists of melanoma inhibitor of apoptosis (ML-IAP). *Biochemistry* **42**, 8223–8231 (2003).
39. T. K. Oost, C. Sun, R. C. Armstrong, A.-S. Al-Assaad, S. F. Betz, T. L. Deckwerth, H. Ding, S. W. Elmore, R. P. Meadows, E. T. Olejniczak, A. Oleksijew, T. Oltersdorf, S. H. Rosenberg, A. R. Shoemaker, K. J. Tomaselli, H. Zou, S. W. Fesik, Discovery of potent antagonists of the antiapoptotic protein XIAP for the treatment of cancer. *J. Med. Chem.* **47**, 4417–4426 (2004).
40. R. A. Kipp, M. A. Case, A. D. Wist, C. M. Cresson, M. Carrell, E. Griner, A. Wiita, P. A. Albiniak, J. Chai, Y. Shi, M. F. Semmelhack, G. L. McLendon, Molecular targeting of inhibitor of apoptosis proteins based on small molecule mimics of natural binding partners. *Biochemistry* **41**, 7344–7349 (2002).
41. S. Deng, R. Marmorstein, Protein N-terminal acetylation: Structural basis, mechanism, versatility, and regulation. *Trends Biochem. Sci.*, S0968-0004(20)30202-4 (2020).
42. F. Frottin, A. Martinez, P. Peynot, S. Mitra, R. C. Holz, C. Giglione, T. Meinnel, The proteomics of N-terminal methionine cleavage. *Mol. Cell. Proteomics* **5**, 2336–2349 (2006).
43. O.-K. Song, X. Wang, J. H. Waterborg, R. Sternglanz, An N^{α}-acetyltransferase responsible for acetylation of the N-terminal residues of histones H4 and H2A. *J. Biol. Chem.* **278**, 38109–38112 (2003).
44. K. Hole, P. van Damme, M. Dalva, H. Aksnes, N. Glomnes, J. E. Varhaug, J. R. Lillehaug, K. Gevaert, T. Arnesen, The human *N*-alpha-acetyltransferase 40 (hNaa40p/hNatD) is conserved from yeast and N-terminally acetylates histones H2A and H4. *PLOS ONE* **6**, e24713 (2011).
45. P. Van Damme, R. Evjenth, H. Foyn, K. Demeyer, P.-J. De Bock, J. R. Lillehaug, J. Vandekerckhove, T. Arnesen, K. Gevaert, Proteome-derived peptide libraries allow detailed analysis of the substrate specificities of N^{α}-acetyltransferases and point to hNaa10p as the post-translational actin N^{α}-acetyltransferase. *Mol. Cell. Proteomics* **10**, M110.004580 (2011).
46. A. Drazic, H. Aksnes, M. Marie, M. Boczkowska, S. Varland, E. Timmerman, H. Foyn, N. Glomnes, G. Rebowski, F. Impens, K. Gevaert, R. Dominguez, T. Arnesen, NAA80 is actin's N-terminal acetyltransferase and regulates cytoskeleton assembly and cell motility. *Proc. Natl. Acad. Sci. U.S.A.* **115**, 4399–4404 (2018).
47. M. Goris, R. S. Magin, H. Foyn, L. M. Myklebust, S. Varland, R. Ree, A. Drazic, P. Bhambra, S. I. Støve, M. Baumann, B. E. Haug, R. Marmorstein, T. Arnesen, Structural determinants and cellular environment define processed actin as the sole substrate of the N-terminal acetyltransferase NAA80. *Proc. Natl. Acad. Sci. U.S.A.* **115**, 4405–4410 (2018).
48. B. P. Eckelman, G. S. Salvesen, The human anti-apoptotic proteins cIAP1 and cIAP2 bind but do not inhibit caspases. *J. Biol. Chem.* **281**, 3254–3260 (2006).
49. F. L. Scott, J.-B. Denault, S. J. Riedl, H. Shin, M. Renatus, G. S. Salvesen, XIAP inhibits caspase-3 and -7 using two binding sites: Evolutionarily conserved mechanism of IAPs. *EMBO J.* **24**, 645–655 (2005).
50. E. N. Shiozaki, J. Chai, D. J. Rigotti, S. J. Riedl, P. Li, S. M. Srinivasula, E. S. Alnemri, R. Fairman, Y. Shi, Mechanism of XIAP-mediated inhibition of caspase-9. *Mol. Cell* **11**, 519–527 (2003).
51. S. Fulda, D. Vucic, Targeting IAP proteins for therapeutic intervention in cancer. *Nat. Rev. Drug Discov.* **11**, 109–124 (2012).
52. S. Fulda, Smac mimetics to therapeutically target IAP proteins in cancer. *Int. Rev. Cell Mol. Biol.* **330**, 157–169 (2017).
53. S. T. Beug, C. E. Beauregard, C. Healy, T. Sanda, M. St-Jean, J. Chabot, D. E. Walker, A. Mohan, N. Earl, X. Lun, D. L. Senger, S. M. Robbins, P. Staeheli, P. A. Forsyth, T. Alain, E. C. La Casse, R. G. Korneluk, Smac mimetics synergize with immune checkpoint inhibitors to promote tumour immunity against glioblastoma. *Nat. Commun.* **8**, 14278 (2017).
54. Z. Wang, Z. Wang, J. Guo, Y. Li, J. H. Bavarva, C. Qian, M. C. Brahimi-Horn, D. Tan, W. Liu, Inactivation of androgen-induced regulator ARD1 inhibits androgen receptor acetylation and prostate tumorigenesis. *Proc. Natl. Acad. Sci. U.S.A.* **109**, 3053–3058 (2012).
55. C.-F. Lee, D. S.-C. Ou, S.-B. Lee, L.-H. Chang, R.-K. Lin, Y.-S. Li, A. K. Upadhyay, X. Cheng, Y.-C. Wang, H.-S. Hsu, M. Hsiao, C.-W. Wu, L.-J. Juan, hNaa10p contributes to tumorigenesis by facilitating DNMT1-mediated tumor suppressor gene silencing. *J. Clin. Invest.* **120**, 2920–2930 (2010).
56. H. Xu, B. Jiang, L. Meng, T. Ren, Y. Zeng, J. Wu, L. Qu, C. Shou, *N*-α-acetyltransferase 10 protein inhibits apoptosis through RelA/p65-regulated MCL1 expression. *Carcinogenesis* **33**, 1193–1202 (2012).
57. T. Arnesen, D. Gromyko, F. Pendino, A. Ryningen, J. E. Varhaug, J. R. Lillehaug, Induction of apoptosis in human cells by RNAi-mediated knockdown of hARD1 and NATH, components of the protein *N*-α-acetyltransferase complex. *Oncogene* **25**, 4350–4360 (2006).
58. C. H. Yi, D. K. Sogah, M. Boyce, A. Degterev, D. E. Christofferson, J. Yuan, A genome-wide RNAi screen reveals multiple regulators of caspase activation. *J. Cell Biol.* **179**, 619–626 (2007).
59. H.-K. Kim, R.-R. Kim, J.-H. Oh, H. Cho, A. Varshavsky, C.-S. Hwang, The N-terminal methionine of cellular proteins as a degradation signal. *Cell* **156**, 158–169 (2014).

60. F. Pietrocola, L. Galluzzi, J. M. Bravo-San Pedro, F. Madeo, G. Kroemer, Acetyl coenzyme A: A central metabolite and second messenger. *Cell Metab.* **21**, 805–821 (2015).
61. R. T. Timms, Z. Zhang, D. Y. Rhee, J. W. Harper, I. Koren, S. J. Elledge, A glycine-specific N-degron pathway mediates the quality control of protein *N*-myristoylation. *Science* **365**, eaaw4912 (2019).
62. S.-E. Ong, B. Blagoev, I. Kratchmarova, D. B. Kristensen, H. Steen, A. Pandey, M. Mann, Stable isotope labeling by amino acids in cell culture, SILAC, as a simple and accurate approach to expression proteomics. *Mol. Cell. Proteomics* **1**, 376–386 (2002).
63. S.-E. Ong, M. Mann, Mass spectrometry–based proteomics turns quantitative. *Nat. Chem. Biol.* **1**, 252–262 (2005).
64. E. Mastrangelo, F. Cossu, M. Milani, G. Sorrentino, D. Lecis, D. Delia, L. Manzoni, C. Drago, P. Seneci, C. Scolastico, V. Rizzo, M. Bolognesi, Targeting the X-linked inhibitor of apoptosis protein through 4-substituted azabicyclo[5.3.0]alkane smac mimetics. Structure, activity, and recognition principles. *J. Mol. Biol.* **384**, 673–689 (2008).
65. O. Kleifeld, A. Doucet, A. Prudova, U. auf dem Keller, M. Gioia, J. N. Kizhakkedathu, C. M. Overall, Identifying and quantifying proteolytic events and the natural N terminome by terminal amine isotopic labeling of substrates. *Nat. Protoc.* **6**, 1578–1611 (2011).
66. B. Metz, G. F. A. Kersten, P. Hoogerhout, H. F. Brugghe, H. A. M. Timmermans, A. de Jong, H. Meiring, J. ten Hove, W. E. Hennink, D. J. A. Crommelin, W. Jiskoot, Identification of formaldehyde-induced modifications in proteins: Reactions with model peptides. *J. Biol. Chem.* **279**, 6235–6243 (2004).
67. X. Zhang, J. Ye, P. Hojrup, A proteomics approach to study *in vivo* protein N^{α}-modifications. *J. Proteomics* **73**, 240–251 (2009).
68. N. C. Hubner, A. W. Bird, J. Cox, B. Splettstoesser, P. Bandilla, I. Poser, A. Hyman, M. Mann, Quantitative proteomics combined with BAC TransgeneOmics reveals in vivo protein interactions. *J. Cell Biol.* **189**, 739–754 (2010).
69. J. Cox, M. Mann, MaxQuant enables high peptide identification rates, individualized p.p.b.-range mass accuracies and proteome-wide protein quantification. *Nat. Biotechnol.* **26**, 1367–1372 (2008).
70. J. Cox, M. Y. Hein, C. A. Luber, I. Paron, N. Nagaraj, M. Mann, Accurate proteome-wide label-free quantification by delayed normalization and maximal peptide ratio extraction, termed MaxLFQ. *Mol. Cell. Proteomics* **13**, 2513–2526 (2014).
71. S. Tyanova, T. Temu, P. Sinitcyn, A. Carlson, M. Y. Hein, T. Geiger, M. Mann, J. Cox, The Perseus computational platform for comprehensive analysis of (prote)omics data. *Nat. Methods* **13**, 731–740 (2016).
72. C. A. Schneider, W. S. Rasband, K. W. Eliceiri, NIH Image to ImageJ: 25 years of image analysis. *Nat. Methods* **9**, 671–675 (2012).
73. H.-C. Yen, Q. Xu, D. M. Chou, Z. Zhao, S. J. Elledge, Global protein stability profiling in mammalian cells. *Science* **322**, 918–923 (2008).
74. A. Bachmair, D. Finley, A. Varshavsky, In vivo half-life of a protein is a function of its amino-terminal residue. *Science* **234**, 179–186 (1986).

Acknowledgments: We thank M. Metz and A. Brockmeyer for help with the maintenance of the MS equipment; J. B. Mueller for the gift of MS columns; T. Grossmann, C. Still, and S. Gentz for initial synthesis of peptides; G. Ossolengo for help with preparation of the anti-AcCDC20 antibody; and D. Bier for help with the purification of XIAP. The His-tag BIR domain constructs and XIAP FL were gifts of E. Mastrangelo and M. Bolognesi. **Funding:** A.M. gratefully acknowledges funding by the Max Planck Society, the European Research Council (ERC) Advanced Investigator Grant RECEPIANCE (proposal 669686) and the DFG's Collaborative Research Centre (CRC) 1093. T.B. was supported by a grant from the Friedrich-Baur Stiftung. **Author contributions:** F.M. performed pull-down, immunoblot, and apoptosis assays. A.F. performed fluorescence polarization assays. C.P. performed the N-terminal enrichment in HeLa cells. R.C.d.S. assisted and analyzed flow cytometry experiments. K.B.R. wrote the PeptideSearchTool App. T.B. performed pull-down and in vitro ubiquitination assays, MS data acquisition, and analysis of MS data. A.M. and T.B. designed experiments and wrote the manuscript. **Competing interests:** The authors declare that they have no competing interests. **Data and materials availability:** All data needed to evaluate the conclusions in the paper are present in the paper and/or the Supplementary Materials. The MS proteomics data have been deposited to the ProteomeXchange Consortium via the PRIDE partner repository with the dataset identifier PXD021815. Additional data related to this paper may be requested from the authors.

Submitted 18 May 2020
Accepted 24 November 2020
Published 15 January 2021
10.1126/sciadv.abc8590

Citation: F. Mueller, A. Friese, C. Pathe, R. C. da Silva, K. B. Rodriguez, A. Musacchio, T. Bange, Overlap of NatA and IAP substrates implicates N-terminal acetylation in protein stabilization. *Sci. Adv.* **7**, eabc8590 (2021).